Journal of Computational Interdisciplinary Sciences (2010) 1(3): 233-239

ISSN 1983-8409
http://epacis.org

A Biologically Motivated Fuzzy-like Measure for Complex Structures Perception

Thalita Biazzuz Veronese[1] and Maurício Pozzobon Martins[2]

Manuscript received on February 26, 2010 / accepted on April 2, 2010

ABSTRACT

In contrast to the perceptual capability of artificial systems, the biological perception of spatial patterns is a continuous cognitive process. In particular, the visual system of primates has a space-variant nature where the resolution is high on the fovea and decreases continuously to the periphery of the visual field. Moreover, the pattern perception and recognition may change, also continuously, when orientation and depth changes. An interesting aspect is that the perceptual performance needs to increase when the structure in recognition gets more complex in terms of irregular spatial contents (asymmetries). Based on these properties, we introduce a computational measurement procedure where the asymmetries are "continuously" quantified using intersections among partially fuzzy images. The asymmetries are quantified using the first gradient moment from the Gradient Pattern Analysis methodology. In this application, the first gradient moment is a fuzzy parameter whose fuzzy deviation is set in the same level of biological perceptual uncertainty. The performance of our approach is tested over texture variation perception in SAR (Synthetic Aperture Radar) images and the results show that this measure can be useful for real-time machine navigation and, in a more general sense, for biologically motivated morphology research.

Keywords: Computer vision, fuzzy logic, complex structures perception.

[1] LAC-INPE, São José dos Campos, SP, Brazil. E-mail: thalitabv@gmail.com

[2] IEAv-DCTA, São José dos Campos, SP, Brazil. E-mail: mauricio@ieav.cta.br

1 INTRODUCTION

For a computational vision device, the perception performance with moving and changing view areas of textures and objects is essential to perform dynamical pattern recognition and functional orientation [1]. In biologically inspired artificial pattern perception (and recognition), the characterization level should change, in a continuous way, when orientation and depth change [2]. In this paper, a partial continuous perception process is proposed in terms of a fuzzy-like reduced set of interconnected patterns whose orientation is previously determined in order to quantify the perceptual accuracy of a virtual robotic eye.

For a given extended image $n \times m$, a sequence of sub-image scenes represents the dynamical information to aid in understanding an oriented motion, but increases the amount of data to be processed by the system. Fortunately, research in dynamic-scene analysis has shown that the recovery of information in many cases is easier in a dynamical approach than in a static one [1]. In this preliminary approach we are interested in the MCSO category (Moving Camera and Stationary Objects), most important for navigation applications.

In our approach, an original image is masked using a sequence of sub-images that represents the motion of a virtual camera. The most discrete motion is represented by a set of few sub-images that can be detected by its level of asymmetry represented in the gradient field of the image. The partial continuous motion (inspired in a biological mode) is represented by a set of interconnected images having a common area defined from a superposition of width τ. The asymmetry profile of this partial continuously fuzzy-like set is then compared to the discrete one.

In next Section the data and methodology are introduced. The results and concluding remarks are in Sections 3 and 4, respectively.

2 DATA AND METHODOLOGY

2.1 SAR Images and Fuzzy-like Sequences

The image used in this paper was obtained in 2004 September 13, by the SAR (Synthetic Aperture Radar) sensor of SIVAM's (Amazon Vigilance System - http://www.sivam.gov.br) remote sensing aircraft. The collection region is placed in the city of Machadinho d'Oeste - RO, Brazil. The SIVAM's SAR sensors have, beyond other characteristics, ability of imaging in two wave lengths (bands X and L), multipolarization in band L (HH, W, HV and VH), interferometric way in band X and space resolution varying of 1.8 to 18m. Figure 1(a) shows an image of size 192×64 pixels, where many texture patterns are visible. The discrete mode (Mode D) is illustrated in Figure 1(b). The discrete covered mask contains three 64×64 windows, representing the discrete motion perception process (from the left to the right or vice-versa). The partial continuous mode – biologically motivated – (Mode B) is represented in Figure 1(c). The partial continuous mask contains four 64×64 windows, representing the continuous perception process (from the left to the right or vice-versa). It is defined from three superposing areas, each one of width $\tau = 22$ pixels. This area represents a perceptual sensitivity greater than 20% of the visual angle. This sensitivity is compatible to the biological continuous visual perception of primates. Actually, the visual system of primates has a space-variant nature where the resolution is high on the fovea and decreases continuously to the periphery of the visual field.

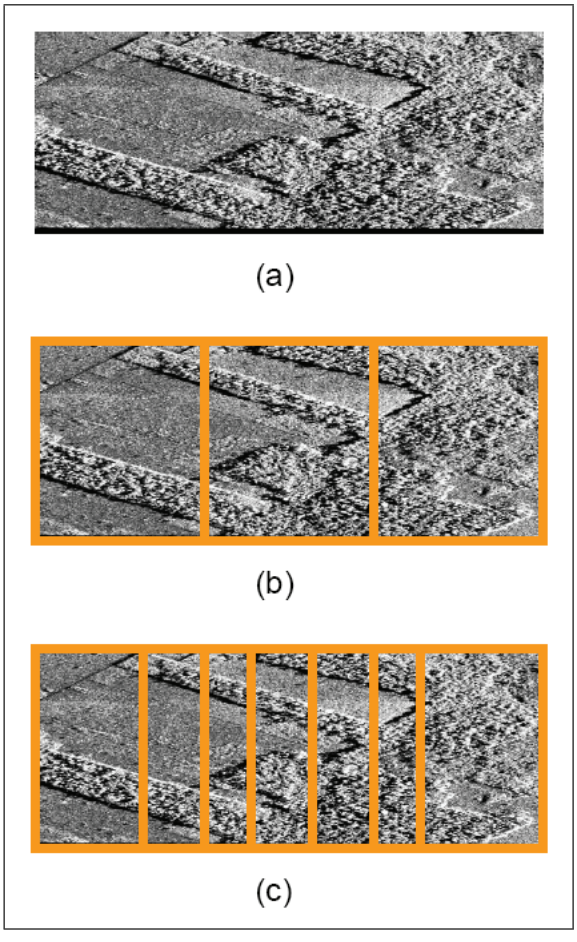

Figure 1 – (a) An arbitrary SAR image composed by 192×64 pixels with different textures. (b) The discrete covered mask containing three 64×64 windows representing the discrete perception process (from the left to the right or vice-versa). (c) The partial continuous mask containing four 64×64 windows representing the continuous-like perception process (from the left to the right or vice-versa).

The τ width in the fuzzy-mask shown in Figure 1(c) can be easily calculated from the formula:

$$\tau = \lceil Ln^2/T \rceil - n \,, \tag{1}$$

where T is total number of longitudinal pixels (here, $T = 192$), n is the size of the discrete mask (here, $n = 64$) and L is the number of images necessary to exactly cover T. Considering a generic view angle for the best perception, τ represents the confidence area where the perception is still high in a continuous visual motion.

2.2 The Asymmetry Coefficient

Usually the characterization of irregular structures observed in digital images is performed on the absolute values of the amplitude in each pixel. However, the computational method Gradient Pattern Analysis is straightforward and brings some advantages on the traditional methodologies [3]. The gradient asymmetry coefficient G_A is intrinsically calculated on the amplitude differences (local gradients) given by the image gradient pattern [11]. As the first gradient moment is very sensitive to small changes in the phase and modulus of each gradient vector, it can distinguish complex variability patterns even when they are very similar and consist of a low amount of vectors.

Thus, a given scalar field of fluctuations (a $n \times m$ image, for example) can be represented as a gradient field having N_V vectors corresponding to the pixel-pixel local gradient (see Appendix).

In this context, for a given $n \times m$ global fluctuation pattern, the gradient asymmetry coefficient is computed by means of the asymmetric amplitude fragmentation operator [4, 5], that measures the symmetry breaking of a given fluctuation lattice by means of quantity:

$$G_A = \frac{N_C - N_V}{N_V} \,, \tag{2}$$

where $N_V > 0$ is the total number of asymmetric vectors and N_C is the number of Delaunay connections among them. The geometric connection among the fluctuations is generated by a Delaunay triangulation taking the middle points of the asymmetric vectors as vertices (Figure 2(b)). Figure 3 shows a schematic diagram as a short algorithmic description of gradient asymmetry coefficient calculus.

Due to the possible changes in the phases of each fluctuation (a vector in the gradient lattice), the parameter N_V is very sensitive in detecting local asymmetric fluctuations (as irregular textures in images) on the gradient lattice [4, 5]. Moreover, for the composition of irregular textures with the same level of probability distribution, the G_A parameter has high sensitivity in distinguishing both images from the mixture frame. Thus, we use this operation in order to characterize the detection path during our virtual camera motion taking into account the two modes (discrete and partially continuous) shown in Figure 4. As we have $L = 3$ for mode D and $L = 4$ for mode B, G_A is obtained as a function of L, the character of each sub-frame. The values of $G_A(L)$ for modes D and B are shown in the next Section.

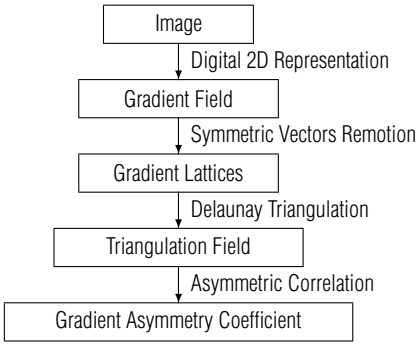

Figure 2 – Steps for calculating gradient asymmetry coefficient.

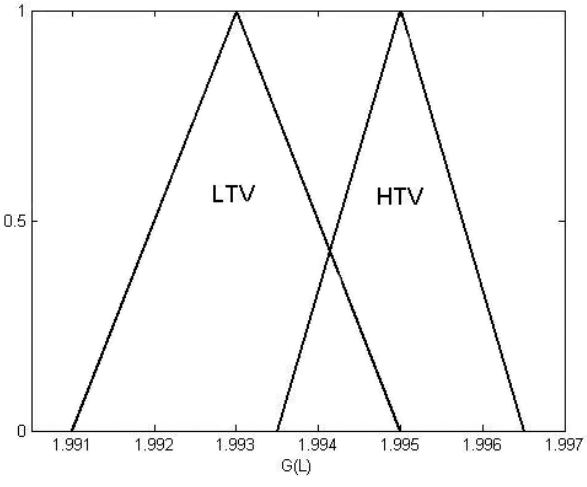

Figure 3 – Categories, based on the $G_A(L)$ measures, for texture variability of the fuzzy-like frames: Low Texture Variability (LTV) and High Texture Variability (HTV).

3 A FUZZY ASYMMETRY

Many applications of fuzzy sets and fuzzy logic can be found in robotics and pattern recognition fields [1, 6]. In this work, our fuzzy asymmetry will be defined in a similar way, as represented in Figure 4, with two fuzzy categories related to the texture variability of the analysed sub-image. The idea is to quantify this variability by associating the values obtained for $G_A(L)$ to membership functions defined in each fuzzy category. For now, the sub-images

can have, up to a membership degree, low or high texture variability.

4 RESULTS

The asymmetry profiles for modes D and B are shown in Figure 4. Once the standard deviation of $G_A(L)$ is less than 10^{-4} for $n = 64$, from these curves one can distinguish with great accuracy both modes. Due to the fuzzy area between the images in mode B, the values of G have shown that the fuzzy-like images have more asymmetries in their respective gradient field than the discrete images. Also, the biological mode (Mode B) is more nonlinear than the Mode D. This behavior is expected due to the high sensitivity of the parameter G_A.

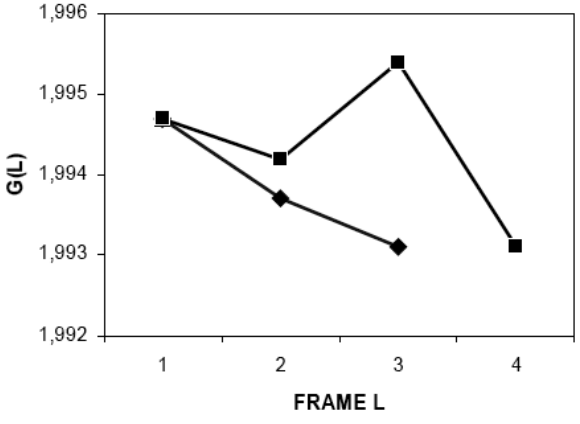

Figure 4 – Comparison between the asymmetries profiles of Mode D (shortest inferior one, represented by three measurements) and Mode B (the superior curve represented by four measurements).

It is important to stress that the profiles showed in Figure 4 are representative of textures, without any explicitly morphological characterization. In order to be used by subsequent tasks like 2-D and 3-D morphological classification [7, 8], the meaning of asymmetries in the fuzzy width τ must be defined taking into account the asymmetries of object (or areas) contours. For this purpose the GPA technique has been adapted for one dimensional manifolds as lines, curves and projections for different morphologies [9].

5 CONCLUDING REMARKS

Detection of changes in two successive frames of a sequence is a very important step for many applications. In this preliminary work we have shown that the asymmetry coefficient is a good measure for fuzzy-like sub-images representing a scene where different textures must be detected approximately in the same way of an animal visual perception. Having introduced the T/τ fuzzy like mask concept, the next step in this research is to consider a fuzzy-like vertical depth in this approach. From a complete description of partial continuous perception for textures one can address the problem of massive computation considering high resolution images visualized in more realistic color systems. Such improvements will bring the mode C closer to a truly biological mode. Further research will be also developed taking into account the asymmetry profiles as a new parameter set to be used in supervised learning processes for intelligent robotic cameras.

ACKNOWLEDGMENT

Authors thank to CNPq and Força Aérea Brasileira (FAB) for financial support.

APPENDIX

Gradient Pattern Analysis

A square gradient lattice, composed by N vectors, is defined as the lattice $\sqrt{N} \times \sqrt{N}$ where each lattice point has a gradient vector identified by its norm and phase. For a square matrix of amplitudes M_N (composed by $\sqrt{N} \times \sqrt{N} = N$ pixels) the respective gradient square lattice is written as $\nabla M = [M_X, M_Y]$. The GPA gradient operation on M returns the X and Y components of the two-dimensional numerical gradient. M_X and M_Y are the differences d_X and d_Y in horizontal and vertical directions, respectively. The spacing between points in each direction is assumed to be one. The first output M_X is always the gradient along the 2nd dimension of M, going across columns. The second output M_Y is always the gradient along the 1st dimension of M, going across rows. The algorithm for $\nabla M = [M_X, M_Y]$ takes forward differences on left and right edges and takes centered differences on interior points. The procedure to calculate the gradient pattern from an exemple of elementary matrix is shown in Figure 5.

Gradient patterns can be symmetric or asymmetric according to the GPA formalism. The distribution of vectors at each meshpoint in the lattice can contain many with the same magnitude, within a small error, and these will be symmetric pairs if they have opposite orientations, and asymmetric pairs otherwise.

Let us consider two generic vectors $\mathbf{V}_a$ and $\mathbf{V}_b$ belonging to the gradient lattice set. $\mathbf{V}_a$ and $\mathbf{V}_b$ are vectorially symmetric if $\mathbf{V}_a = -\mathbf{V}_b$ so that the resulting vector $R_{a+b} = \mathbf{V}_a + \mathbf{V}_b = \mathbf{0}$ (the null vector). In computational terms, the resulting vector is null within a given tolerance for Euclidian norms ϵ_v (that assigns to each vector the length of its arrow) and phases ϵ_ϕ (that assigns to each vector the angle of its orientation). In the original algo-

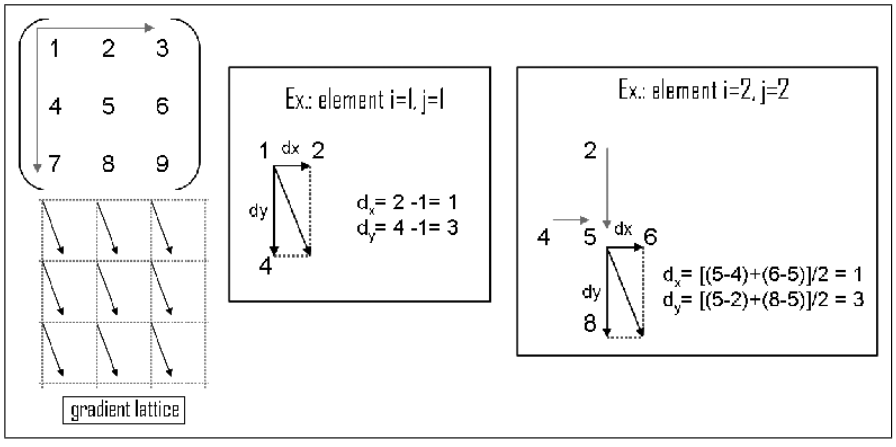

Figure 5 – Example of an elementary M_9 (3×3) matrix and its respective asymmetric gradient pattern. Calculation for the matrix elements (1,1) and (2,2) are ilustrated as examples.

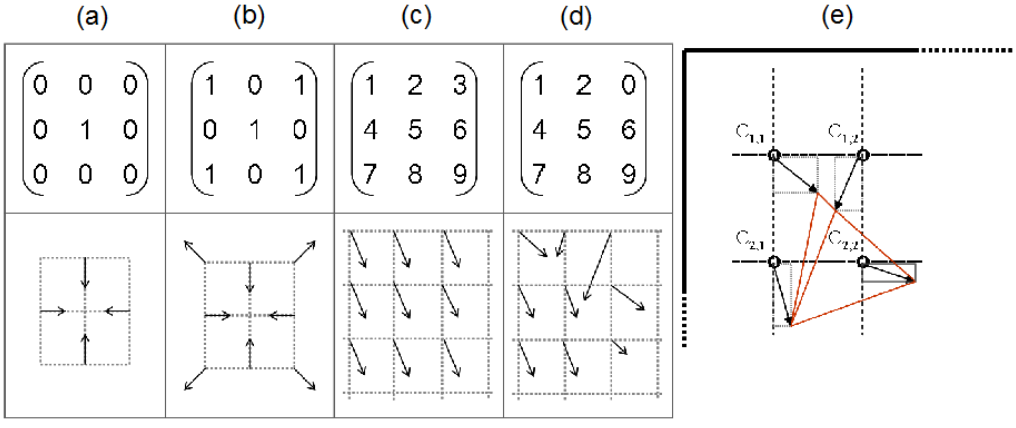

Figure 6 – Examples of elementary M_9 (3×3) matrices and their respective symmetric (a and b) and asymmetric gradient patterns (c and d). (e) Example ofthe local Delaunay triangulation among vectors in a generic gradient lattice.

rithms, both tolerances are chosen equal to one tenth of standard deviation of norms and phases.

Removing every pair of symmetric vectors from the gradient lattice, the gradient pattern is symmetric when all possible resulting vectors R_{a+b} are null. Otherwise, the gradient pattern is asymmetric. Examples of elementary M_9 (3×3) symmetric and asymmetric gradient patterns are shown in Fig. A2, where the (a) and (b) have corresponding symmetric patterns with all $R_{a+b} = 0$, while the (c) and (d) are asymmetric with $N_V = 9$, the number of non-null resulting vectors in the gradient lattice.

Figure 6 shows that symmetry breaking in a gradient pattern can be detected following changes in the norm and phase of each vector in the lattice. As shown in Figure 6(d), an efficient geometrical method to follow at the same time both changes is the triangulation among the vectors arrowheads.

Using the parameter N_V (number of asymmetric vectors) and the number of connections among them, given by N_C, the gradient asymmetry for a given gradient pattern can be numerically characterized. Note that, in a given triangulation performed on the gradient lattice, each triangle is as equilateral as possible and obeys the empty circle criterion which allows us to construct the triangulation pattern directly from the sample set. In computational geometry, the triangulation pattern among the gradient vectors is generated calculating the Delaunay triangulation among them, from where the computation of the convex hull of a finite set of points is straighforward [10], hence allowing the computation of the parameter N_C. Figure 7 shows the respective Delaunay triangulation meshes for the asymmetric gradient patterns of Figure 5. Note that the parameter N_C increases when the structural asymmetry of the gradient pattern becomes

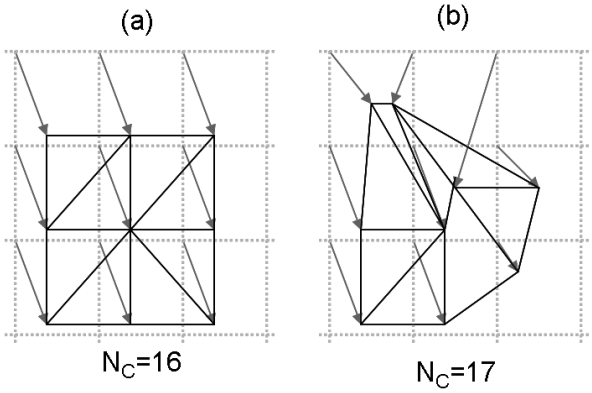

Figure 7 – Triangulation patterns for the asymmetric gradient lattices of Fig. A2: (a) for the asymmetric gradient lattice on the left and (b) for the asymmetric gradient lattice on the right.

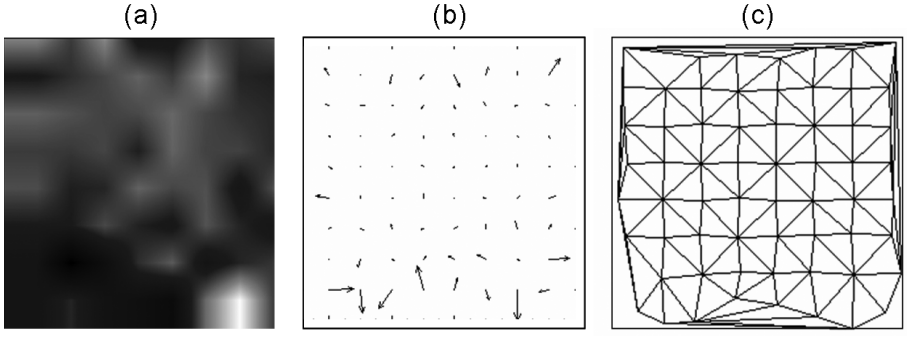

Figure 8 – Gradient pattern analysis of an 8×8 arbitrary matrix: (a) the original digital image; (b) its asymetric gradient field and (c) its corresponding triangulation field resulting $G_A = 1.8065$.

more irregular (or disordered).

As shown by [3], an interesting property of the gradient triangulation pattern is that $N_C > N_V$ and the difference $N_C - N_V$ will increase with N_V as

$$\lim_{N_V \to \infty} (N_C - N_V) \approx 2N_V.$$

Therefore, the so-called gradient asymmetry coefficient $G_A = \frac{N_C - N_V}{N_V}$ tends asymptotically to 2. This asymptotic regime implies a very high accuracy of the value G_A to compare different gradient patterns of the same size.

Figure 8(a) shows an small image as an example so that its corresponding square matrix has a 8×8 size. The corresponding gradient pattern is shown in Figure 8(b) and represents the asymmetric gradient lattice obtained after removing all symmetric pairs from the gradient pattern. The respective triangulation pattern is shown in Figure 8(c). Note that the asymmetry information intrinsically appears in the triangulation lattice range.

It has been shown from several applications that GPA is applied in some cases where a given variable (or amplitude) $A(s)$ measured as a function of the discrete domain (s) shows evidence of fine nonlinear variations (or scaling irregular roughness). Besides its properties for asymmetric pattern classification, the essential characteristic of GPA applications we consider here is that the measure G_A is fitted to gradient lattices either to compare slightly different irregular patterns or to characterize pattern formation in terms of gradient asymetries. Consequently, GPA is a fine comparative analysis basically based on geometric and scaling criteria that should be adopted to compare data having the same size (number of points or pixels) where the associated amplitude values are in the same quantitative domain. Otherwise the resulting gradient asymmetries can not be compared.

REFERENCES

[1] JAIN R, KASTURI R & SCHUNCK BG. 1995. Machine Vision, McGraw-Hill, Inc.

[2] WANDELL BA. 1995. Foundations of Vision, Sunderland, Massachusetts.

[3] ROSA RR, SHARMA AS & VALDIVIA JA. 1999. Int. J. Mod. Phys. C, 10: 147–163.

[4] ASSIREU AT, ROSA RR, VIJAYKUMAR NL, LORENZETTI JA, REMPEL EL, RAMOS FM, ABREU SÁ SL, BOLZAN MJA & ZANANDREA A. 2002. Physica D, 168(1): 397–403.

[5] ROSA RR, KARLICKÝ M, VERONESE TB, VIJAYKUMAR NL, SAWANT HS, BORGAZZI AI, DANTAS MS, BARBOSA EBM, SYCH RA & MENDES O. 2008. Gradient pattern analysis of short solar radio bursts, Advances in Space Research, 42: 844–851.

[6] RAO VB & RAO HV. 1993. C++ Neural Networks and Fuzzy Logic, Mit Press, New York.

[7] SOILLE P. 1999. Morphological Image Analysis, Springer.

[8] TRUCCO E & VERRI A. 1998. Introductory Techniques for 3-D Computer Vision, Prentice Hall, New Jersey.

[9] ASSIREU AT et al. 2004. Aplicação do Operador de Fragmentação Assimétrica (FA) na caracterização de controles geomorfológicos em reservatórios hidroelétricos, Revista Brasileira de Geociências, 34(4): 501–508.

[10] TSAI VJD. 1993. Delaunay triangulations in TIN creations: an overview and a linear-time algorithm. Int. J. Geogr. Inf. Syst. 7: 501–524.

[11] GRADIENT PATTERN ANALYSIS, Wikipedia.
http://en.wikipedia.org/wiki/Gradient_pattern_analysis.